Nuclear Engineering and Technology 55 (2023) 3506–3513

Contents lists available at ScienceDirect

Nuclear Engineering and Technology

journal homepage: www.elsevier.com/locate/net

Original Article

Evaluation of neutron attenuation properties using helium-4 scintillation detector for dry cask inspection

Jihun Moon [a], Jisu Kim [b], Heejun Chung [b], Sung-Woo Kwak [b], Kyung Taek Lim [c, *]

[a] The Nuclear Safety and Security Commission, Seoul, Republic of Korea
[b] Korea Institute of Nuclear Non-proliferation and Control, Daejeon, Republic of Korea
[c] Quantum and Nuclear Engineering, Sejong University, Seoul, Republic of Korea

ARTICLE INFO

Article history:
Received 26 September 2022
Received in revised form
25 April 2023
Accepted 22 June 2023
Available online 18 July 2023

Keywords:
S670e
Helium-4 detector
dry cask
Neutron shielding
Neutron detection

ABSTRACT

In this paper, we demonstrate the neutron attenuation of dry cask shielding materials using the S670e helium-4 detector manufactured by Arktis Radiation Ltd. In particular, two materials expected to be applied to the TN-32 dry cask manufactured by ORANO Korea and KORAD-21 by the Korea Radioactive Waste Agency (KORAD) were utilized. The measured neutron attenuation was compared with our Monte Carlo N-Particle Transport simulation results, and the difference is given as the root mean square (RMS). For the fast neutron case, a rapid decline in neutron counts was observed as a function of increasing material thickness, exhibiting an exponential relationship. The discrepancy between the experimentally acquired data and simulation results for the fast neutron was maintained within a 2.3% RMS. In contrast, the observed thermal neutron count demonstrated an initial rise, attained a maximum value, and exhibited an exponential decline as a function of increasing thickness. In particular, the discrepancy between the measured and simulated peak locations for thermal neutrons displayed an RMS deviation of approximately 17.3–22.4%. Finally, the results suggest that a minimum thickness of 5 cm for Li-6 is necessary to achieve a sufficiently significant cross-section, effectively capturing incoming thermal neutrons within the dry cask.

1. Introduction

In South Korea, Spent Nuclear Fuel (SNF) from pressurized water reactors (PWRs) have been stored in on-site pool storage facilities, but their maximum capacity is expected to be reached in less than a decade [1]. On this subject, it is necessary to introduce an intermediate storage facility before permanent disposal, for example, dry cask storage. In particular, after transferring and sealing the SNF in a dry cask, the IAEA requires the integrity of the SNF inside the dry casks to be verified. One reasonable solution in safeguard and verification technology is a non-destructive test. Devices such as Passive Gamma Emission Tomography (PGET) are used to inspect SNF in a pool before loading. However, this method suffers from self-attenuation due to the high activity of individual spend fuel rods [2]. To solve this problem, neutron tomography has been considered an alternative non-destructive solution for verifying dry cask storage [3]. A detector based on helium-3 gas, which has a high thermal neutron cross-section, is a golden standard for many neutron detection applications. Although a helium-3 detector has been a 'gold standard' in neutron detection for a decade, a challenge of the helium-3 shortage is becoming significant [4,5], and moderation is still required to detect the fast neutrons with helium-3 proportional counters. On the other hand, helium-4 gas is being actively studied as a possible alternative to helium-3 gas detectors. Helium-4 is a stable isotope of helium commonly found on Earth. In particular, the neutron cross-section near 1 MeV is higher than that of the helium-3, so a moderator is not required, which is an advantage over fast neutron detection. Numerous studies have been conducted based on helium-4 scintillation detection: for example, detecting fission signals and monitoring SNF storage facilities [6,7], non-destructive testing of mixed oxide reactor fuel [8], and fast-neutron dose monitoring [9]. A proportional counter based on helium-4 gas is also used to detect high-energy neutrons due to its linearity; however, it has the disadvantage of limited detection efficiency [10]. Nevertheless, using helium-4 for neutron detection offers the advantage of knowing the energy of incident neutrons.

* Corresponding author. Quantum and Nuclear Engineering, Sejong University, 209 Neungdong-ro, Gwangjin-gu, Seoul, 05006, Republic of Korea.
E-mail address: kl2548@sejong.ac.kr (K.T. Lim).

https://doi.org/10.1016/j.net.2023.06.039

Recently, the Korea Institute of Nuclear Non-proliferation and Control (KINAC) developed an inspection prototype based on neutron detection to safeguards and verify dry storage facilities projected in South Korea [11]. This study aimed to assess the feasibility of passive neutron measurement for inspecting dry storage facilities for SNF that is likely to be introduced into Korea [11,12]. In particular, the prototype was built using six Arktis S670e helium-4 detectors, each having 180-bar pressure of helium-4 gas. The inner wall of the Arktis S670e detector is coated with Li-6 so that it can also detect thermal neutrons. Furthermore, S670e has multiple silicon photomultipliers (SiPMs) placed inside the cylinder to detect scintillation light [9]. In a previous work, a Transnuclear-32 (TN-32) dry storage cask with a 1/10th-scale thickness was manufactured, and a different arrangement of Cf-252 sources was used to evaluate the prototype [11]. However, the previous work did not evaluate the shielding properties due to the shielding materials inside the dry cask [13,14]; the thickness of the model cask was too thin, at 1.1 cm.

The neutron attenuation due to the shielding material should be considered as it can degrade the image quality acquired via the tomographic approach. Indeed, many studies have evaluated the properties of neutron shielding materials in the past [15–17]; however, there has been no attempt to measure the neutron attenuation using the off-the-shelf Arktis S670e detector. In addition, some studies have investigated S670 or S670e models, but most relied on dismantling the analog readout board instead of using the factory default [18–24]. Lastly, few studies have evaluated the neutron attenuation properties of shielding materials expected to be used in the TN-32 model manufactured in South Korea.

In this work, we evaluated the neutron attenuation properties of shielding materials using the S670e helium-4 detector. In particular, we used two different composites for shielding materials that are expected to be applied to the TN-32 dry cask manufactured by ORANO Korea and KORAD-21 by the Korea Radioactive Waste Agency (KORAD). The shielding materials were custom-cut with identical thicknesses to measure the fast/thermal neutron counts as a function of material thickness. Furthermore, we tested the statistical variation in the off-the-shelf S670e detector before the shielding evaluation to assess its reliability and limitations. Lastly, a MCNP6 simulation in an identical experimental environment was carried out for comparison.

2. Materials and methods

The reliability and limitation of the S670e helium-4 detector were first tested. The S670e detector used in this work was identical to that of the helium-4 detector in the previous work [11]. In particular, the statistical variation in the recorded counts due to repeated measurements, detector incident-angle, and long-duration operation of the detector was evaluated. Then, the neutron shielding properties of the shielding materials used in developing TN-32 and KORAD-21 are likely to be adopted as the dry cask for storing SNF from PWR reactors in South Korea [12,25]. Two types of shielding materials, each with different thicknesses, were placed between the Cf-252 neutron emitter and S670e detector to evaluate the neutron attenuation with respect to different thicknesses.

The Arktis S670e is filled with helium-4 gas at 180 bar, and its inner wall is coated with Li-6. The basic operation principle of the detector is as follows: when the fast neutron interacts with a helium-4 atom, it is excited and ionizes nearby helium-4 atoms. Eventually, the helium-4 atom is excited through a series of processes, and the excited helium-4 atom is returned to the ground state by emitting approximately 18,000 photons per 1 MeV deposited by neutrons [18]. As for thermal neutrons, an α-particle and tritium with energies of 2.05 MeV and 2.72 MeV are generated through a $^{6}Li(n, a)^{3}H$ reaction. These generated photons are then detected by SiPMs embedded inside the detector. In addition, the active volume of S670e is divided into three segments, each having four pairs of SiPMs. The detected neutrons are determined to be either fast neutrons or thermal neutrons via time-over-threshold (ToT) values set by the detector [9,11].

At KINAC, a 1/10th-scale TN-32 model was built, and neutrons were measured for distances ranging from 13–27 cm between the source and the helium-4 detector array [11]. The distance varied depending on the neutron source configuration. Thus, we chose two different values for the neutron attenuation evaluation to account for the minimum and maximum separation distances, i.e., 13 cm and 27 cm. In addition, we chose the middle segment for measuring the detector characteristics and neutron attenuation properties because the fabricated shielding blocks were not large enough to cover the entire active volume. Moreover, there was a slight variation in the measured neutron counts among the three segments [24]. As for discriminating between the fast and thermal neutrons, the factory default setting was used for ToT values for all measurements [11]. We did not consider the influence of the gamma-ray interactions because S670e has a high gamma-rejection ratio [26]. The neutron spectrum of the Cf-252 source and the neutron cross-section of He-3, He-4, and Li-6 are shown in Fig. 1 [17,27].

2.1. Testing the S670e helium-4 detector

Three tests were performed to assess the statistical variation in the measured fast/thermal neutron counts due to the detector's repeatability, measurement direction, and long-duration operation. We first demonstrated the repeatability of the detector under identical conditions. The experimental setup is shown in Fig. 2. The S670e detector was fixed at the end of a flat table. Ruler tape was used at the center of segment 1 (henceforth, the middle segment) to measure the distance between the source and the detector and the thickness of the shielding materials. The Cf-252 source was placed 27-cm away from the detector center. For the measurement, we recorded it for 5 min and repeated it 11 times.

Second, we evaluated the change in neutron counts concerning the direction of S670e. As mentioned before, each segment of S670e had four pairs of SiPMs attached to PCB boards embedded inside the detector, which could cause a variation in the light collection efficiency depending on the incident direction of the detector. To access the directionality, we performed 5-min measurements for different angles by rotating the detector from 0° to 330° at 30° intervals, as shown in Fig. 3.

Lastly, we investigated the possible statistical variation due to the continuous operation of the detector. The reason is that the safeguards prototype developed at KINAC is intended to measure fast/thermal neutrons coming out from the dry storage facility. As a result, the measurements may take more than a few hours, depending on the cask design and SNF cooling time. On the other hand, the SiPMs used to measure the scintillation light in S670e are sensitive to temperature. In particular, the temperature-compensation mechanism does not apply for S670 and S670e models, as noted by Arktis Ltd [26]. Thus, if any, the change in the neutron counts due to the long-duration operation of the detector should be considered. In this experiment, we recorded the fast/thermal counts from 5 to 480 min.

Lastly, we investigated the possible statistical variation due to the continuous operation of the detector because the safeguards prototype developed at KINAC is intended to measure fast/thermal neutrons coming out of a dry storage facility. For this, the measurements may take more than a few hours, depending on the cask

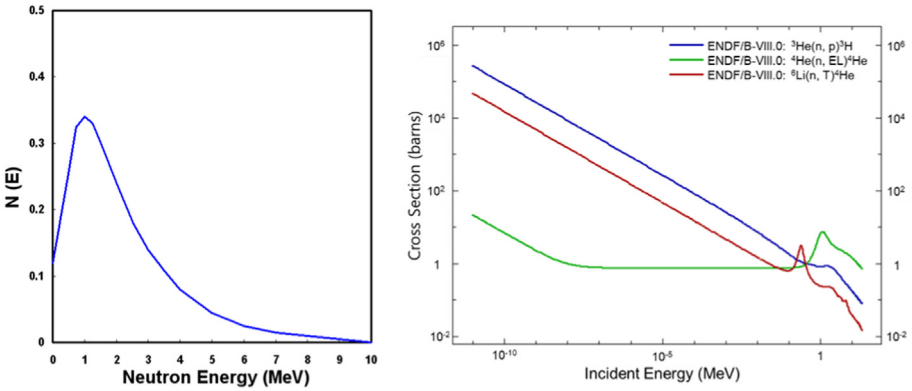

Fig. 1. The emission spectrum of Cf-252 [17] and the cross-section of He-3, He-4, and Li-6 [27].

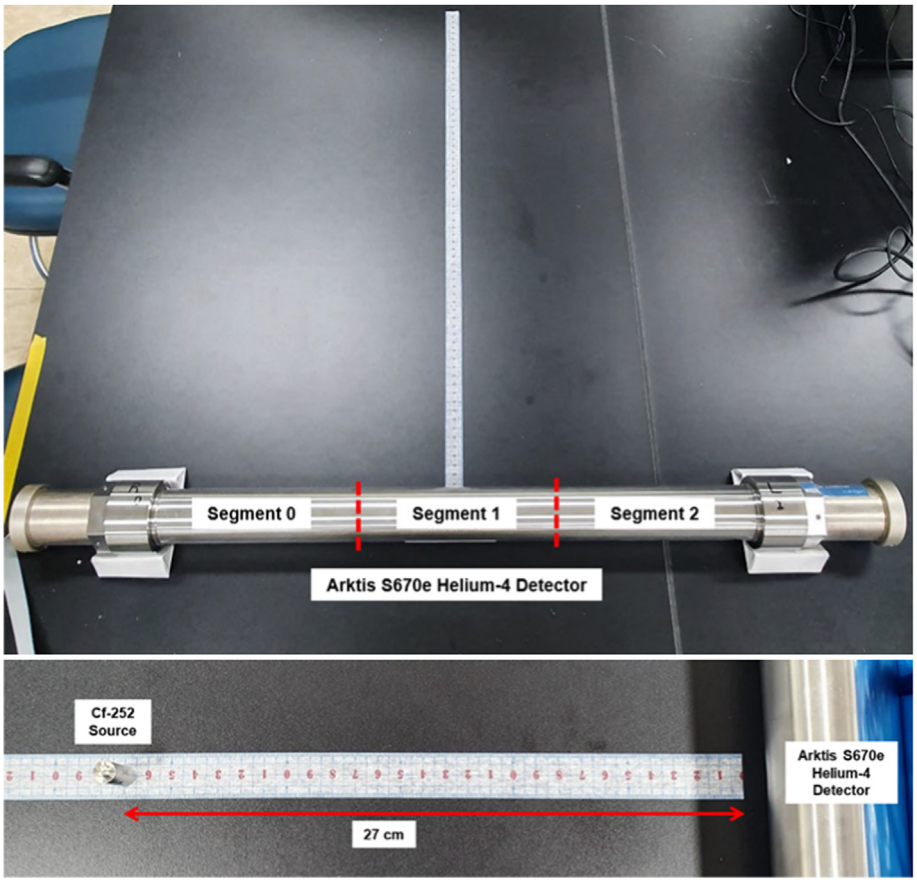

Fig. 2. Experimental setup for S670e repeatability test.

design and SNF cooling time. On the other hand, the SiPMs used to measure the scintillation light in S670e are sensitive to temperature. In particular, the temperature-compensation mechanism does not apply for S670 and S670e models, as noted by Arktis Ltd [26]. Thus, if any, the change in the neutron counts due to the long-duration operation of the detector should be considered. In this experiment, we recorded the fast/thermal counts from 5 to 480 min.

2.2. Evaluation of the neutron attenuation properties

In cooperation with ORANO-Korea and BRNC (Bridge btwn Radwaste & Clearance), we obtained samples of shielding blocks used for building TN-32 and KORAD-21 dry casks. Two types of shielding blocks (Resin and RANO shield) and their corresponding compositions are shown in Fig. 4 and Table 1. We fixed all conditions other than the shielding blocks so that the main variable in this experiment would be the material compositions and the block thicknesses. The experimental setup is shown in Fig. 5. The measurement was performed using the S670e model and Cf-252 source, similar to Fig. 2. The main difference was that we placed shielding blocks with different thicknesses between the source and the detector to evaluate the neutron attenuation properties. In particular, we measured the neutron counts by increasing the shielding

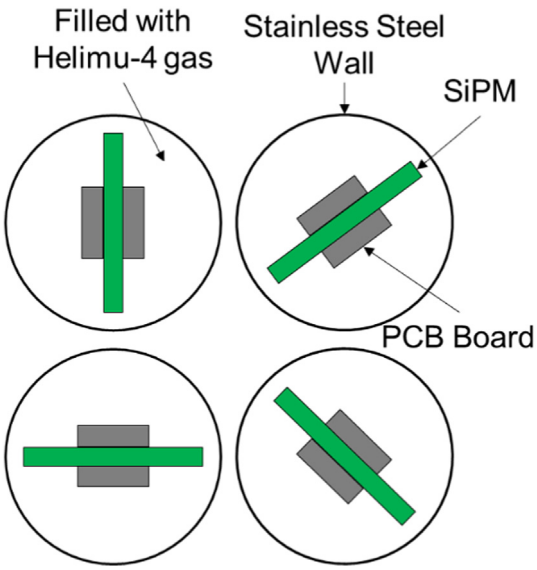

Fig. 3. Schematic diagram of SiPMs in S670e detector [9].

thickness in the order of 1, 2, 3, 4, 5, 7, 9, 12, 15, and 20 cm. Note that the maximum shielding thickness was 12 cm for the 13-cm case.

Furthermore, MCNP6.2 modeling was performed to compare it with the experimental results [28]. The details of MCNP modeling are as follows: first, the Arktis S670e model used in this experiment measures both fast neutrons and thermal neutrons simultaneously, so the simulation must reflect this. The radius of the active volume of helium-4 gas is 2.608 cm, the height is 60.828 cm, and it is filled 100% with helium-4. Assuming that the molar mass of helium-4 is 4.003 g/mol, the filling pressure is 180 atm, the average temperature is 24.7 °C, and the derived helium-4 density is equal to 0.029481 g/cm^3. In the case of Li-6, an approximately 10-μm thick coating was placed on the detector's inner wall. We assumed that Li-6 has a density of 1.51 g/cm^3 with 100% material composition. As for the detector enclosure, a typical stainless steel SUS304 was used for the modeling. Instead of modeling the SiPM, we modeled so as to count the reaction by the reactants helium-4 gas and Li-6 layer via the F4 tally. Using the F4 tally and FM card to each helium-4 and Li-6 layer in the active volume, the neutrons that scattered with helium-4 were classified as fast neutrons, and the ^{6}Li(n, a)^{3}H reactions were classified as thermal neutrons. In this case, the ENDF/B-VII.0 and ENDF/B-VII.1 libraries were used for each material's nuclear reaction cross-sectional area. In addition, the F4 tally was also divided into three parts to reflect the divided segments. The neutron source was simulated with the Watt fission spectrum of Cf-252. Lastly, the particle history was set not to exceed the maximum error of 1%.

Fig. 4. TN-32 Resin (Left) KORAD-21 RANO shield (Right).

Table 1
Material compositions of TN-32 resin and RANO shield.

TN-32 resin	MASS(g)	RANO shield	Mass(g)
Al	118.20	H	16.16
C	52.61	B-10	0.62
O	70.08	B-11	2.74
H	4.42	C	112.42
B-10	43.86	Al	47.78
B-11	48.23	O	27.58
		Zn-64	54.19
		Zn-66	31.52
		Zn-67	4.66
		Zn-68	21.60
		Zn-70	0.74
Sum	337.40	Sum	320.00

3. Results and discussions

3.1. Testing the S670e Helium-4 detector

Fig. 6 shows the change in fast and thermal neutron counts of the S670e helium-4 detector for the repeated measurements under identical conditions. We took 11 measurements (i.e., cycles), and each cycle was recorded for 5 min. The average counts for fast and thermal neutrons were 654.2 and 251.3, respectively. The variations in the measured fast and thermal neutron counts were within their standard deviation. However, if we look at the 95% confidence interval, some values fell outside the confidence interval. As for the fast neutrons, the maximum deviation was about 9.4%, while the deviation was more significant for thermal neutrons, i.e., approximately 10.5%.

Fig. 7 demonstrates the statistical variation in the measured fast and thermal neutron count of the S670e detector due to the different incident angles. As shown in Fig. 3, the detector was

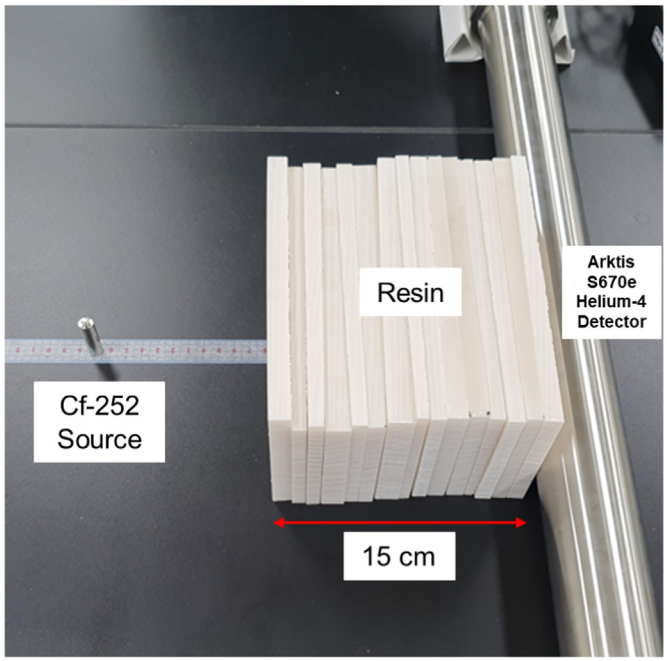

Fig. 5. Experimental setup for evaluating neutron attenuation properties.

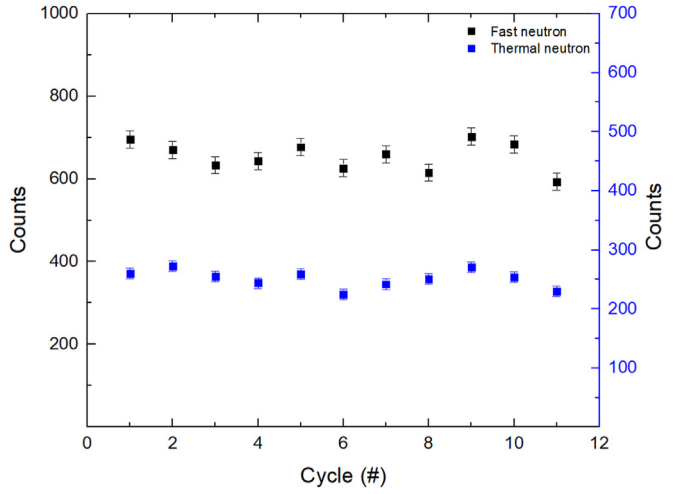

Fig. 6. Fluctuation in the neutron counts as a function of measurement cycle.

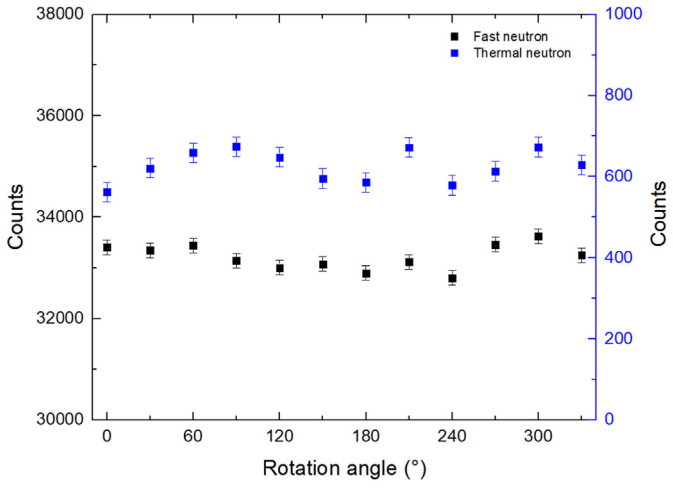

Fig. 7. Fluctuation in the neutron counts as a function of detector rotation angle.

rotated from 0° to 330° at 30° intervals. The fast and thermal neutrons were recorded at each incident angle for 5 min. The fluctuation was less than 1.3% for the fast neutrons, and the variation was approximately 0.5–10.2% for the thermal neutron. If we consider the statistical fluctuation due to the measurement repetition seen in Fig. 6, the influence of the detector's axial orientation is negligible. Therefore, it would be reasonable to believe that the measured fast and thermal neutron counts are uniform with respect to the detector incident angle.

Fig. 8 shows the change in the measured fast and thermal neutron counts of S670e due to the 8-h operation. In general, the results were similar to the previous evaluations where the statistical variations in the fast neutron were less than those of thermal neutrons; the average deviation was approximately 0.6% and 4.2% for the fast and thermal neutrons, respectively. Note that there was an abrupt change in the temperature of the detector in the early measurements. This was due to the quick temperature increase in the SiPM, which is commonly observed in many semiconductor devices. Nevertheless, the deviation in the measured neutron counts was not as dramatic as in the detector temperature. The deviation in the measured counts was most significant for the first 30 min, but then it smoothed out as the operation time increased. Considering the fluctuation found in the repeated measurements (Fig. 6) and rotation angle (Fig. 7), the temperature dependency of SiPMs had a negligible effect on the S670e detector performance, which also suggests that the helium-4 gas filled inside the cylinder chamber is sufficient to stabilize the detector temperature to a certain level, e.g., 28 °C.

3.2. Evaluation of the neutron attenuation properties

Based on the S670e characterization, we evaluated the neutron attenuation properties of fast and thermal neutrons using two different shielding materials. The fast and thermal neutron attenuations with respect to shielding material thicknesses are shown in Figs. 9 and 10, respectively. The experimental results are represented as black squares, whereas the MCNP simulation results are depicted as red circles. We normalized the count values of measurement and simulation results for comparison. In particular, we calculated the root mean square (RMS) differences between the measured and simulated values using equation (1). Assuming the measured quantities as true values, the RMS increased with an increasing difference between the true and simulated values. That is, the discrepancy between the true and simulated results increased with an increasing RMS value. The RMS values are reported in Tables 2 and 3.

$$x_{rms} = \sqrt{\frac{x_1^2 + x_2^2 + \bullet\bullet\bullet + x_n^2}{n}} \quad where \quad x_i = x_{measured} - x_{simulated}$$

equation (1)

For the fast neutrons, the measured and simulated counts decreased with an increasing shield thickness for both the resin and the RANO shield regardless of the distance. The RMS values reported for the fast neutrons were about 1.5–2.3% for both cases. In contrast, thermal neutrons increased with an increasing shield thickness at the beginning for both distances (see the thermal neutrons of Figs. 9 and 10). Then, at a certain thickness, the thermal neutrons begin to decrease with an increasing shield thickness, following the expected attenuation behavior.

Many neutrons emitted from Cf-252 have an energy range of 0.5–5 MeV. In case of helium-4, a neutron has the highest interaction probability at near 1 MeV (see Fig. 1). This agrees with the observed results where fast neutron counts were at the maximum when there were no shielding materials present between the source and the detector. On the other hand, the presence of a moderator is essential for Li-6 to detect neutrons emitted from the Cf-252 source (see Fig. 1). As the thickness of the TN-32 resin and the RANO shield increased, the fast neutrons modulated to lower energies but not enough to interact with Li-6. However, as the thickness increased, the moderated neutrons reached lower energies sufficient to be captured by Li-6. Thus, there is a certain thickness of Li-6 in which the cross-section becomes significant enough to capture the incoming thermal neutrons.

When the distance between the source and detector was 27 cm, the peak appeared at 5 cm and 7 cm for the measured and simulated thermal neutron counts, respectively. When the distance was at 13 cm, the peaks of both the resin and the RANO shield were observed at near 6 cm for the measured result. On the other hand, the peaks were observed at near 9 cm in the simulation. Due to these discrepancies, the RMS values of the thermal neutron ranged from 17.3 to 22.4%, as shown in Tables 2 and 3 The absence of concrete structures surrounding the measurement room and the influence of neutron scattering could have contributed to the observed differences.

We also noted that there was a difference in the thermal neutrons between the TN-32 resin and the RANO shield. In particular,

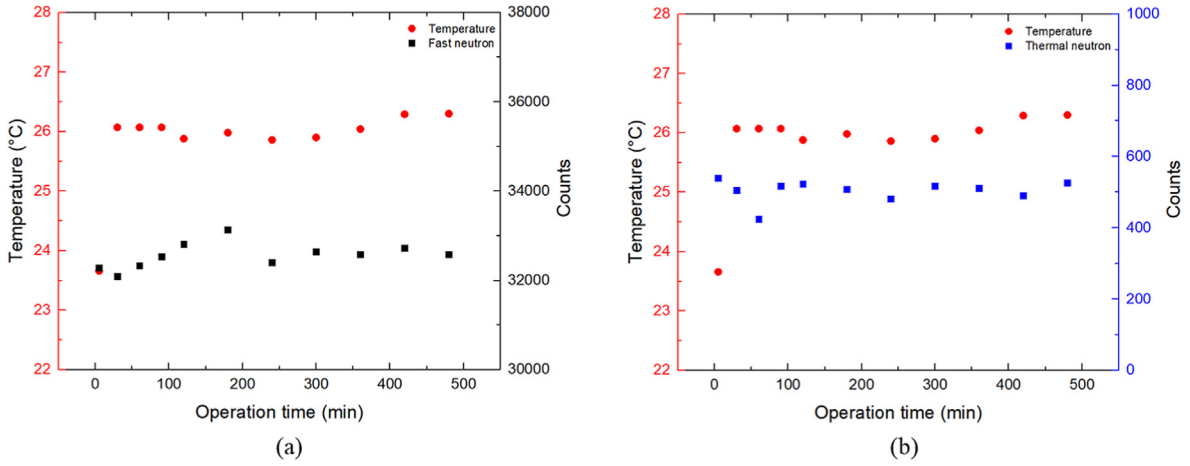

Fig. 8. Fluctuation in the neutron counts as a function of long-duration operation for the (a) fast neutron and (b) thermal neutron.

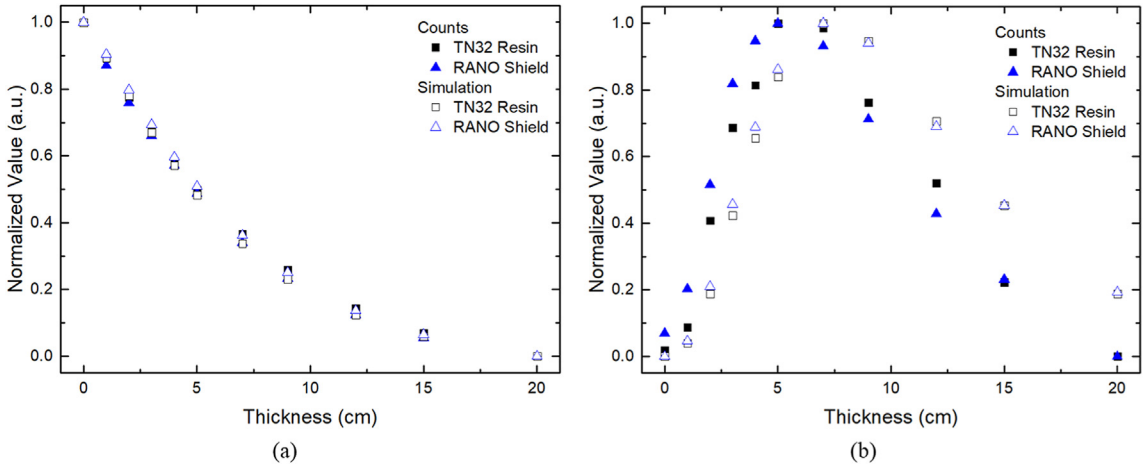

Fig. 9. Measured and simulated counts as a function of shielding thickness for the (a) fast neutron and (b) thermal neutron. The distance from the source to detector is set as 27 cm.

the counts were lower for the resin before the peak, whereas the attenuation became greater for the RANO shield beyond the peak. When we compare the material composition of the TN-32 resin and the RANO-shield, we see that the elements Al, C, and O are most common in both shields, but the resin has more significant quantities of B while the RANO-shield contains Zn. Thus, we suspect that this composition difference of B and Zn between the two shielding materials caused the discrepancy in the neutron attenuation behaviors.

4. Conclusion

We demonstrated the neutron shielding properties of two materials that are expected to be used to construct dry casks for South Korea's PWR SNF. We utilized an off-the-shelf S670e detector manufactured by Arktis Radiation Ltd that was used in the safeguard prototype developed at KINAC. Before the shielding characterization, we tested the S670e helium-4 detector to assess the statistical variation in neutron counting due to repeated measurements, incident-angle dependence, and long-duration operation. The maximum fluctuation due to 11 consecutive measurements was 9.4% for fast neutrons, whereas the maximum fluctuation was 10.5% for thermal neutrons in all three experiments. We also confirmed that the temperature dependency of SiPMs was negligible for an 8-h-long operation.

We then evaluated the neutron shielding properties of two shielding materials by measuring the fast and thermal neutron counts as a function of material thickness. Also, the measured values were compared with simulation results, and the difference was denoted in terms of RMS. The fast neutron counts decreased exponentially with increasing thicknesses with a difference of less than 2.3% RMS. As for thermal neutrons, however, there was a threshold for the material thickness in which the moderated neutrons began attenuating with increasing thickness. The trends in the measured and simulated results were similar, but the peak locations differed, with a deviation from 17.3% to 22.4% RMS. We suspect the difference between the measured and simulated values is possibly due to the absence of concrete structures surrounding the measurement room and the influence of neutron scattering. Furthermore, the observed variation in neutron attenuation properties between the two shielding materials can likely be attributed to their boron and zinc composition differences.

This research investigated the degree to which shielding materials can influence neutron image reconstruction using the safeguard prototype developed at KINAC. In a previous study, the shield thickness was 1.1 cm, so its importance was negligible. However, a minimum thickness of 5 cm for Li-6 is necessary to achieve a sufficiently significant cross-section, effectively capturing incoming thermal neutrons within the dry cask. Also, the shield thickness is at least 11 cm thick in an actual cask. Thus, a correction factor

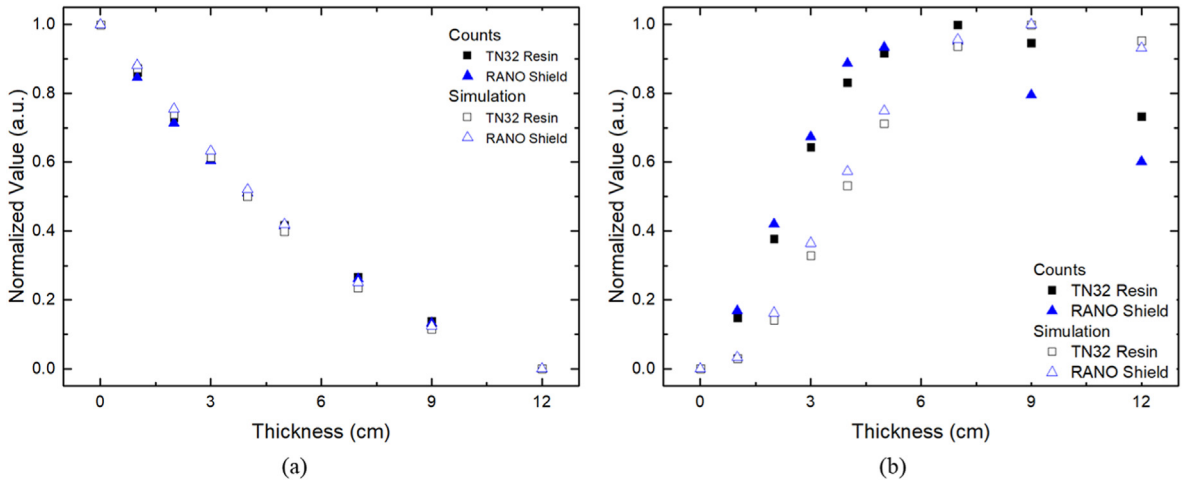

Fig. 10. Measured and simulated counts as a function of shielding thickness for the (a) fast neutron and (b) thermal neutron. The distance from the source to detector is set as 13 cm.

Table 2
The RMS of measured and simulated counts for TN-32 Resin and RANO shield at the distance of 27 cm.

Neutron	Fast		Thermal	
Shielding Material	Resin	RANO	Resin	RANO
RMS (%)	1.460	2.314	17.295	22.421

Table 3
The RMS of measured and simulated counts for TN-32 Resin and RANO shield at the distance of 13 cm.

Neutron	Fast		Thermal	
Shielding Material	Resin	RANO	Resin	RANO
RMS (%)	1.662	2.020	19.230	21.895

should be addressed to utilize the developed prototype for on-site testing. In particular, the modification of shielding thickness in the model cask could provide a more accurate prediction of the attenuated neutron flux at the dry cask surface due to the shielding in an actual cask. Furthermore, the results also imply the S670e He-4 detector can exhibit reliable outputs at long-term operation despite the well-known temperature dependence of SiPMs.

In future research, we plan to: develop and optimize the model cask that resembles a real TN-32 cask, optimize detection windows for fast and thermal neutron discrimination, and evaluate the He-4 detector's suitability for on-site neutron measurements of a dry cask.

Declaration of competing interest

The authors declare that they have no known competing financial interests or personal relationships that could have appeared to influence the work reported in this paper.

Acknowledgments

This work was supported by the Nuclear Safety Research Program through the Korea Foundation Of Nuclear Safety (KoFONS) using financial resources granted by the Nuclear Safety and Security Commission (NSSC) of the Republic of Korea (No. 2106016) and by the faculty research fund of Sejong University in 2022 of the Republic of Korea.

References

[1] C. Braun, R. Forrest, Consideration regarding ROK spent nuclear fuel management options, Nucl. Eng. Technol. 45 (2013) 427–438.
[2] M. Fang, et al., Quantitative imaging and automated fuel pin identification for passive gamma emission tomography, Sci. Rep. 11 (2021) 2442.
[3] A.J. Hurd, R.T. Kouzes, Why new neutron detector materials must replace helium-3, The European Physical Journal Plus 129 (2014) 236.
[4] The High Neutron Mapping System In-Field Measurements in 2008, Los Alamos National Laboratory, 2009.
[5] F. Piscitelli, G. Mauri, A. Laloni, R. Hall-Wilton, Verification of He-3 proportional counters' fast neutron sensitivity through a comparison with He-4 detectors, The European Physical Journal Plus 135 (2020) 577.
[6] J.M. Lewis, R.P. Kelley, D. Murer, K.A. Jordan, Fission signal detection using helium-4 gas fast neutron scintillation detectors, Appl. Phys. Lett. 105 (2014), 014102.
[7] A. Enqvist, Used Fuel Storage Monitoring Using Helium-4 Scintillation Fast Neutron Detectors and Neutron Spectral Analysis, United States, 2019, p. 76.
[8] D. Murer, et al., MOX Assay Using He-4 Scintillation Detectors, SPIE, 2012.
[9] P. Tancioni, et al., Fast neutron dose rate monitoring using off the shelf Helium-4 scintillation detectors, The International Journal of Nuclear Safeguards and Nonproliferation 62 (2021) 35–42.
[10] M. Manolopoulou, et al., Studies on the response of ^{3}He and ^{4}He proportional counters to monoenergetic fast neutrons, Nucl. Instrum. Methods Phys. Res. 562 (2006) 371–379.
[11] K.T. Lim, et al., The feasibility of passive neutron measurement for dry storage safeguards approach, IEEE Trans. Nucl. Sci. 69 (2022) 1331–1335.
[12] W. Choi, et al., Current Status of Korean Multi-Modal Transportation Test (MMTT), Transactions of the Korean Nuclear Society, 2020.
[13] TN-32 Dry Storage Cask System Safety Evaluation Report, Transnuclear, Inc, 2000.
[14] S.R. Greene, J.S. Medford, S.A. Macy, Storage and Transport Cask Data for Used Commercial Nuclear Fuel, United States, 2013.
[15] A.S. Mollah, G.U. Ahmad, S.R. Husain, Measurements of neutron shielding properties of heavy concretes using a Cf-252 source, Nucl. Eng. Des. 135 (1992) 321–325.
[16] D.R. McAlister, Neutron Shielding Materials, PG Research Foundation, Inc., 2016.
[17] H. Kang, C. Park, K. Seo, J. Yoon, Evaluation of neutron shielding effects on various materials by using a Cf-252 source, J. Kor. Phys. Soc. 52 (2008) 1744–1747.
[18] R. Chandra, G. Davatz, H. Friederich, U. Gendotti, D. Murer, Fast neutron detection with pressurized ^{4}He scintillation detectors, J. Instrum. 7 (2012). C03035-C03035.
[19] Y. Liang, T. Zhu, A. Enqvist, Timing characterization of helium-4 fast neutron detector with EJ-309 organic liquid scintillator, EPJ Web Conf. 170 (2018), 07005.
[20] R.P. Kelley, et al., Measurement of the fast neutron response for ^{4}He scintillation detectors using a coincidence scattering method, IEEE Trans. Nucl. Sci. 63 (3) (2016) 1600–1607, https://doi.org/10.1109/TNS.2016.2521699.
[21] R.P. Kelley, A. Enqvist, K.A. Jordan, Pulse shape discrimination in helium-4 scintillation detectors, Nucl. Instrum. Methods Phys. Res. 830 (2016) 44–52.
[22] A. Biekert, S.A. Hertel, E. Huebler, J. Lin, H.D. Pinckney, R.K. Romani, A. Serafin, V. Velan, D.N. McKinsey, Nuclear recoil scintillation linearity of a high pressure ^{4}He gas detector, J. Instrum. 14 (2019). P10028-P10028.
[23] R.P. Kelley, L.M. Rolison, J.M. Lewis, D. Murer, T.N. Massey, A. Enqvist, K.A. Jordan, Neutron Response Function Characterization of ^{4}He Scintillation

Detectors, vol. 793, 2015.
[24] C. Barker, T. Zhu, L. Rolison, S. Kiff, K. Jordan, A. Enqvist, Pulse shape analysis and discrimination for silicon-photomultipliers in helium-4 gas scintillation neutron detector, EPJ Web Conf. 170 (2018), 07002.
[25] D. Kook, J. Choi, J. Kim, Y. Kim, Review of spent fuel integrity evaluation for dry storage, Nucl. Eng. Technol. 45 (2013) 115–124.
[26] A.R.D. Ltd, Arktis S670(e) Detector series Operating Manual, Arktis Radiation Detector Ltd., 2018.
[27] D.A. Brown, et al., ENDF/B-VIII.0: the 8th major release of the nuclear reaction data library with CIELO-project cross sections, new standards and thermal scattering data, Nucl. Data Sheets 148 (2018) 1–142.
[28] C.J. Werner (Ed.), MCNP Users' Manual – Code Version 6.2, Los Alamos National Laboratory, 2017.